# Coherent photo- and electroproduction of charmonia on nuclear targets revisited: Green function formalism

J. Nemchik[1,2,*] and J. Óbertová[1,†]

[1]*Czech Technical University in Prague, FNSPE, Břehová 7, 11519 Prague, Czech Republic*
[2]*Institute of Experimental Physics SAS, Watsonova 47, 04001 Košice, Slovakia*

(Received 3 July 2024; accepted 21 August 2024; published 13 September 2024)

We study for the first time the production of charmonia in nuclear ultraperipheral and electron-ion collisions based on a rigorous Green function formalism. Such formalism allows to incorporate properly formation effects (color transparency), as well as the quantum coherence inherent in higher-twist shadowing corrections related to the $|Q\bar{Q}\rangle$ Fock component of the photon. The leading twist gluon shadowing associated with multigluon photon fluctuations is also included within the same formalism. The later effect represents the dominant source of shadowing at midrapidities in the LHC kinematic region, while the reduced effect of quark shadowing leads to a significant modification of differential cross sections $d\sigma/dy$ at forward and/or backwards rapidities. Model calculations for $d\sigma/dy$ are in a good agreement with available ultraperipheral nuclear *Pb-Pb* collisions data on coherent charmonium production at RHIC and the LHC. In addition, we also perform predictions for nuclear effects in the electroproduction of charmonia, which can be verified by new data from electron-ion colliders.

DOI: 10.1103/PhysRevD.110.054015

## I. INTRODUCTION

Charmonium production in photonuclear reactions (photon virtuality $Q^2 \approx 0$) was recently intensively studied in ultraperipheral nuclear *Pb-Pb* collisions (UPC) at the Large Hadron Collider (LHC), as well as in $Au-Au$ UPC collisions at Relativistic Heavy Ion Collider (RHIC). Moreover, future experiments at the planned Electron-Ion Collider (EIC) [1,2] at RHIC will provide us with new data on coherent (elastic), $\gamma^* A \to VA$, and incoherent (quasielastic), $\gamma^* A \to VA^*$ ($A^*$ is an excited state of the A-nucleon system) charmonium $[V = J/\psi(1S), \psi'(2S), \ldots]$, electroproduction ($Q^2 \neq 0$). This allows us to explore manifestations of various nuclear phenomena, such as reduced effects of quantum coherence, color transparency, gluon shadowing, and gluon saturation in new kinematic regions.

The corresponding theoretical studies of nuclear effects are very effective within the light-front (LF) quantum-chromodynamics (QCD) color dipole approach (see e.g., our previous works [3–15]). This formalism allows us to minimize uncertainties in model predictions for quarkonium yields on a proton target as was analyzed in Refs. [16–18] (a comprehensive review on quarkonia phenomenology can be found e.g., in Refs. [19–21]). Such a reduction of theoretical uncertainties is then indispensable for a proper interpretation of phenomena occurring in electronuclear reactions.

In our previous work [15], we performed a detailed analysis of various effects accompanying the heavy quarkonium (HQ) production in UPC. Here we adopted several realistic $Q$-$\bar{Q}$ interaction potentials in the $Q\bar{Q}$ rest frame for calculations of realistic quarkonium wave functions by solving the Schrödinger equation with a subsequent Lorentz boost to high energy. We also adopted several models for the phenomenological dipole cross sections fitted to deep inelastic scattering data. We demonstrated that two main nuclear effects considerably affect the nuclear cross sections. In the RHIC and LHC kinematic regions, at forward and/or backward rapidities, the first of them leads to the reduction of the higher-twist quark shadowing related to the lowest $|Q\bar{Q}\rangle$ Fock state of the photon. The second effect causes the leading twist gluon shadowing, related to higher photon components containing gluons, in the midrapidity region at the LHC energy range.

However, in Ref. [15] the reduced effects of quantum coherence were calculated only approximately. Here, in the high-energy limit of long coherence length, we provided additional corrections via the effective form factors modifying the nuclear cross sections at small and moderate c.m. photon energies, $W \lesssim 30 \div 40$ GeV. Although we have applied a rigorous path integral technique, the corresponding Green function acquired only the analytical harmonic

*Contact author: jan.nemcik@fjfi.cvut.cz
†Contact author: jaroslava.obertova@fjfi.cvut.cz

oscillatory form reducing thus complexity of related calculations. Consequently, we had to use several simplifications, such as quadratic form for the dipole cross section, the harmonic oscillatory form for the light-front $Q$-$\bar{Q}$ interaction potential, and constant nuclear density. Such simplifications cannot be applied for a sufficiently accurate description of data, especially on exclusive electroproduction of 2S-radially-excited heavy quarkonia as was demonstrated in Ref. [16].

In this paper, we revise our previous calculations [15]. We present for the first time the model predictions for charmonium photonuclear and electronuclear production within the full quantum-mechanical description based on a rigorous path integral technique [9]. This allows to obtain more accurate results for reduced effects of quantum coherence beyond simplifications mentioned above. Besides the higher-twist quark shadowing, the leading twist gluon shadowing effects are also calculated within the same Green function formalism [11,13,14,22,23]. This grants a proper and consistent incorporation of both the quantum coherence and color transparency effects. The precise calculation of these phenomena has then a huge impact for a conclusive evidence of saturation effects in UPC [24].

In the most of recent papers (see e.g., Refs. [25,26]), the effect of quantum coherence related to the $Q\bar{Q}$ photon fluctuations is not included properly, as well as shadowing corrections for higher multigluon Fock states of the photon are often neglected or incorporated inaccurately. Recently, new calculations at next-to-leading order (NLO) of exclusive heavy quarkonium production have appeared in the literature (see e.g., Ref. [27]). However, they have been performed only for the proton target and their future extension to nuclear targets is not trivial and may be very complicated for analysis of QCD phenomena. For example, the latest NLO calculations of charmonium production in UPC [28] do not include accurately the quantum coherence effects in the whole rapidity region. This provides another motivation for a more precise and consistent incorporation of nuclear effects in model predictions within the Green function formalism and represents thus the main goal of the present paper. Due to scarcity of data on incoherent charmonium production and complexity of the corresponding calculations within the path integral technique, we will focus mainly on the analyses of model predictions for the elastic production of $J/\psi(1S)$ and $\psi'(2S)$. The diffractive incoherent (quasielastic) production of heavy quarkonia off nuclei will be studied elsewhere.

The paper is organized as follows. In Sec. II we present the basic expression for the rapidity distributions $d\sigma/dy$ of heavy quarkonium production in heavy ion UPC. Section II A is devoted to rigorous Green function formalism, which is applied for description of the coherent process. We verify that such a formalism gives a correct expression in the high-energy limit. At large photon energies we can obtain thus the standard eikonal expression for the coherent quarkonium production cross section. In Sec. II B we analyze the shape of the $Q$-$\bar{Q}$ interaction potential in the LF frame entering the Schrödinger equation for the Green function. We propose a simple prescription how to obtain such LF potentials from various realistic models for the $Q$-$\bar{Q}$ interaction in the $Q\bar{Q}$ rest frame. The resulting full formulas for the nuclear real and virtual photoproduction amplitudes, including also the effects of Melosh spin transformation, can be found in Sec. II C. Since the leading twist shadowing corrections have been analyzed and discussed in our previous works [11,13,14,22,23], in Sec. II D we mention only briefly about the gluon shadowing, which is included in our calculations modifying the nuclear photo- and electroproduction cross sections at large photon energies. In Sec. III, our model calculations within the color dipole approach based on a rigorous path integral technique are compared with available UPC data on charmonium coherent photoproduction off nuclear targets from experiments at RHIC and the LHC. Finally, we also present model calculations of nuclear cross sections in coherent charmonium electroproduction in the kinematic regions covered by experiments at prepared EIC. Our results are summarized and discussed in Sec. IV.

## II. QUARKONIUM PRODUCTION CROSS SECTION IN NUCLEAR ULTRAPERIPHERAL AND ELECTRON-ION COLLISIONS

The photonuclear reaction in a heavy-ion UPC is generated by the photon field of one of the colliding heavy nuclei with a large charge $Z$, which gives rise to strong electromagnetic fields. Then the Weizsäcker-Williams photons are responsible for almost real photoproduction of a vector meson (quarkonium) $V$ with the cross section derived in the one-photon-exchange approximation and expressed in the rest frame of the target nucleus $A$ [29] as

$$k\frac{d\sigma}{dk}=\int d^2\tau\int d^2b\,n(k,\vec{b}-\vec{\tau},y)\frac{d^2\sigma_A(s,b)}{d^2b}+\{y\to -y\}. \tag{2.1}$$

Here the rapidity variable $y=\ln[s/(M_V\sqrt{s_N})]\approx\ln[(2kM_N+M_N^2)/(M_V\sqrt{s_N})]$ with $M_N$ and $M_V$ being the nucleon and vector meson mass, respectively, $\sqrt{s_N}$ is the collision energy and $k$ is the photon energy related to the square of the photon-nucleon center-of-mass (c.m.) energy $W^2=2M_Nk+M_N^2-Q^2\approx s-Q^2$, where $s$ is the lepton-nucleon c.m. energy squared. In Eq. (2.1), the variable $\vec{\tau}$ is the relative impact parameter of a nuclear collision and $\vec{b}$ is the impact parameter of the photon-nucleon collision relative to the center of one of the nuclei. For a collision of identical nuclei with the nuclear radius $R_A$ in UPC, it holds that $\tau>2R_A$ [29].

The projectile nucleus induces the photon flux represented by the variable $n(k,\vec{b})$ in Eq. (2.1) with the following form:

$$n(k,\vec{b}) = \frac{\alpha_{em} Z^2 k^2}{\pi^2 \gamma^2}\left[K_1^2\left(\frac{bk}{\gamma}\right) + \frac{1}{\gamma^2}K_0^2\left(\frac{bk}{\gamma}\right)\right], \quad (2.2)$$

where $\alpha_{em} = 1/137.036$ is the fine-structure constant, $K_{0,1}$ are the modified Bessel functions of the second kind and the Lorentz factor $\gamma = 2\gamma_{col}^2 - 1$ with $\gamma_{col} = \sqrt{s_N}/2M_N$. In heavy ion UPC at the LHC due to very large $\gamma \gg 1$ and small photon virtuality, $-q^2 = Q^2 < 1/R_A^2$, the second term in Eq. (2.2) can be safely neglected since it corresponds to the flux of longitudinally polarized photons.

In the case of the photoproduction and electroproduction of heavy quarkonia at EIC energies, only the corresponding nuclear cross section $d^2\sigma_A(s,b)/d^2b$ is calculated directly, i.e., without the convolution with the photon flux given by Eq. (2.1). Then total cross sections for quarkonium production on nuclear targets are given as an integral over the nuclear impact parameter $b$

$$\sigma_A(s,b) = \int d^2b \frac{d^2\sigma_A(s,b)}{d^2b}. \quad (2.3)$$

### A. Coherent quarkonium production in the Green function formalism

In this paper, we study the elastic production of charmonia on nuclear targets within the LF dipole approach, which has been applied to charmonium photoproduction off nucleons [16,17,30] and nuclei [10,11] before. The corresponding formula for the production cross section has the following form [9]:

$$\frac{d^2\sigma_A^{coh}(s,b)}{d^2b} = |\mathcal{M}^{coh}(s,b)|^2, \quad (2.4)$$

where the amplitude $\mathcal{M}^{coh}(s,b)$ reads

$$\mathcal{M}^{coh}(s,b) = \int_{-\infty}^{\infty} dz \rho_A(b,z) H_1(s,b,z). \quad (2.5)$$

Here $\rho_A(b,z)$ is the nuclear density distribution, for which we employ the realistic Wood-Saxon form with parameters taken from Ref. [31].

In Eq. (2.5), the function $H_1(s,b,z)$ can be expressed within a rigorous path integral technique as

$$H_1(s,b,z) = \int_0^1 d\alpha \int d^2r_1 d^2r_2 \Psi_V^*(\vec{r}_2,\alpha) \times G_{Q\bar{Q}}(z' \to \infty, \vec{r}_2; z, \vec{r}_1)\sigma_{Q\bar{Q}}(r_1,s) \times \Psi_{\gamma(\gamma^*)}(\vec{r}_1,\alpha), \quad (2.6)$$

where $\Psi_V(\vec{r},\alpha)$ is the LF wave function for heavy quarkonium and $\Psi_{\gamma(\gamma^*)}(\vec{r},\alpha)$ is the LF distribution of the $Q\bar{Q}$ Fock component of the quasireal (transversely polarized) or virtual photon. Both wave functions are dependent on the transverse separation $\vec{r}$ of the $Q\bar{Q}$ fluctuation (dipole) and on the variable $\alpha = p_Q^+/p_\gamma^+$, representing the boost-invariant fraction of the photon momentum carried by a heavy quark (or antiquark).

The universal dipole cross section $\sigma_{Q\bar{Q}}(r,s)$ in Eq. (2.6) describes the interaction of the $Q\bar{Q}$ dipole with the nucleon target. Such interaction depends also on the c.m. energy squared $s$, which can be alternatively included also via variable $x = (M_V^2 + Q^2)/s$.

In Eq. (2.6), the function $H_1(s,b,z)$ corresponds to the case when the incident photon produces coherently (elastic scattering) the colorless $Q\bar{Q}$ pair at the point $z$, which then evolves propagating through the nucleus and forms the heavy quarkonium wave function at $z' \to \infty$. The evolution of an interacting $Q\bar{Q}$ pair between points with particular initial and final longitudinal coordinates $z$ and $z'$, and initial and final separations $\vec{r}_1$ and $\vec{r}_2$, is described by the corresponding Green function $G_{Q\bar{Q}}(z',\vec{r}_2;z,\vec{r}_1)$. This Green function satisfies the two-dimensional Schrödinger equation [9,22]

$$i\frac{d}{dz_2}G_{Q\bar{Q}}(z_2,\vec{r}_2;z_1,\vec{r}_1) = \left[\frac{\eta^2 - \Delta_{r_2}}{2k\alpha(1-\alpha)} + V_{Q\bar{Q}}(z_2,\vec{r}_2,\alpha)\right] \times G_{Q\bar{Q}}(z_2,\vec{r}_2;z_1,\vec{r}_1). \quad (2.7)$$

Here the Laplacian $\Delta_{r_2}$ acts on the coordinate $r_2$ and the variable $\eta^2 = m_Q^2 + \alpha(1-\alpha)Q^2$, where $m_Q$ is the heavy quark mass.

Whereas the imaginary part of the LF potential $V_{Q\bar{Q}}(z_2,\vec{r}_2,\alpha)$ in Eq. (2.7) controls the attenuation of the $Q\bar{Q}$ pair in the medium, the corresponding real part describes the interaction between the $Q$ and $\bar{Q}$. The particular shapes of $\mathcal{R}eV_{Q\bar{Q}}(z_2,\vec{r}_2,\alpha)$ are supposed to provide correct LF quarkonium wave functions.

The first kinetic term on the rhs of Eq. (2.7) is responsible for the phase shift of the propagating $Q\bar{Q}$ pair. The corresponding phase factor, $\exp[i\int_{z_1}^{z_2} dz q_L(z)]$, contains the relative longitudinal momentum transfer $q_L(z)$ defined as

$$q_L(z) = \frac{M_{Q\bar{Q}}^2(z) + Q^2}{2k} = \frac{\eta^2 + q_T^2}{2k\alpha(1-\alpha)}, \quad (2.8)$$

where $q_T^2$ is the quark transverse momentum squared and the effective mass squared of the $Q\bar{Q}$ pair reads

$$M_{Q\bar{Q}}^2 = \frac{m_Q^2 + q_T^2}{\alpha(1-\alpha)}. \quad (2.9)$$

Consequently, the *coherence time* [coherence length (CL)] $l_c = 1/q_L$ is contained in the kinetic term of the evolution equation (2.7), taking into account a replacement $q_T^2 \Rightarrow -\Delta_r$. Thus the CL is controlled by dynamically varying $Q\bar{Q}$ effective mass in Eq. (2.7). Its static part can be seen in the last phase shift factor in the Green function (2.27).

For the HQ production, one can use a nonrelativistic limit, $\alpha \sim 0.5$, $M_V^2 \sim 4m_Q^2$ and $m_Q^2 \gg q_T^2$, leading to the following simplified form of the CL:

$$l_c = \frac{2k}{M_V^2 + Q^2}. \tag{2.10}$$

Such a length scale controls the effect of quantum coherence related to the initial-state higher-twist shadowing, which causes suppression as a result of destructive interference of amplitudes associated with interactions on different bound nucleons.

Another phenomenon, accompanying the diffractive photo- and electroproduction of vector mesons (quarkonia) off nuclei, represents the final state absorption of produced quarkonia. It is known as the *color transparency* (CT). Within the color dipole approach (see e.g., Refs. [3–6,8,30,32–34]), the onset of CT is controlled by the $Q\bar{Q}$-size evolution during its propagation through the medium. The estimate of the corresponding time scale controlling such an evolution can be obtained in the rest frame of the nucleus from the uncertainty principle and reads [3,9]

$$t_f = \frac{2k}{M_{V'}^2 - M_V^2}, \tag{2.11}$$

where $M_{V'}$ is the mass of radially excited quarkonium. The time scale $t_f$ in Eq. (2.11) is usually called the *formation time* (formation length) and is also incorporated naturally in a rigorous quantum-mechanical description presented in this work.

In our calculations, we include a small correction in Eq. (2.4) due to the real part of the $\gamma^* N \to VN$ amplitude applying the following replacement [8,35,36],

$$\sigma_{Q\bar{Q}}(r,s) \Rightarrow \sigma_{Q\bar{Q}}(r,s)\left(1 - i\frac{\pi}{2}\Lambda\right),$$
$$\Lambda = \frac{\partial \ln \sigma_{Q\bar{Q}}(r,s)}{\partial \ln s}. \tag{2.12}$$

Note that the amplitude (2.5) is calculated within the Green function formalism without any restriction to CL. In the high-energy limit, when the CL $l_c \gg R_A$ [*long coherence length* (LCL) regime], the Green function acquires a simple form,

$$G_{Q\bar{Q}}(z_2,\vec{r}_2;z_1,\vec{r}_1) \Rightarrow \delta^{(2)}(\vec{r}_1 - \vec{r}_2) \times \exp\left[-\frac{1}{2}\sigma_{Q\bar{Q}}(r_1,s)\int_{z_1}^{z_2} dz \rho_A(b,z)\right]. \tag{2.13}$$

This is the so-called "frozen" approximation, since the transverse sizes of such long-lived $Q\bar{Q}$ photon fluctuations are frozen during propagation through the medium due to the Lorentz time dilation. Consequently, the LCL regime leads to the following simple form of the production amplitude (2.5),

$$\mathcal{M}^{coh}(s,b)\Big|_{l_c \gg R_A} = \int d^2r \int_0^1 d\alpha \Psi_V^*(\vec{r},\alpha) \times \left(1 - \exp\left[-\frac{1}{2}\sigma_{Q\bar{Q}}(r,s)T_A(b)\right]\right) \times \Psi_{\gamma(\gamma^*)}(\vec{r},\alpha), \tag{2.14}$$

where $T_A(b) = \int_{-\infty}^{\infty} dz \rho_A(b,z)$ represents the nuclear thickness function normalized as $\int_0^\infty d^2b T_A(b) = A$, where $A$ is the nuclear mass number.

### B. The $Q$-$\bar{Q}$ potential in the light-front frame

Let's consider the propagation of an interacting $Q\bar{Q}$ pair in a vacuum, where the LF potential $V_{Q\bar{Q}}(z_2,\vec{r}_2,\alpha)$ in Eq. (2.7) contains only the real part. The shape of $\mathcal{R}eV_{Q\bar{Q}}$ is strongly correlated with the form of the quarkonium wave function in the LF frame as discussed below.

We start from the determination of the well-defined quarkonium wave functions in the $Q\bar{Q}$ RF solving the Schrödinger equation with several realistic potentials, such as the standard harmonic oscillatory potential (HO) (see e.g., Ref. [3]), Cornell potential (COR) [37,38], logarithmic potential (LOG) [39], powerlike potential (POW) [40,41], as well as Buchmüller-Tye (BT) potential [42]. All of them give rather close results for the charmonium electroproduction cross sections as is presented in Ref. [30] and the corresponding differences in predictions can be treated as a measure of theoretical uncertainty related to the LF quarkonium distribution function. However, in our calculations we adopt only two of them, denoted as BT and POW, since they provide the best description of available data on proton targets, as was shown in Ref. [16].

As the next step, the nonrelativistic quarkonium wave functions in the $Q\bar{Q}$ RF are boosted to the LF frame using the standard Terent'ev prescription [43] as described in Refs. [16–18,30] (see also Sec. II. B in Ref. [14]). Such a prescription is based on the unjustified assumption that, after performing the Lorentz boost to the LF frame, where the original quarkonium wave function in the RF is expressed in terms of light-front and Lorentz invariant

variables related to two-dimensional transverse momentum $\vec{q}_T$ and $\alpha$, the resulting wave function is also Lorentz invariant. Nevertheless, this Lorentz boosting prescription was tested and verified in Ref. [44] using the Lorentz boosted Schrödinger equation for heavy $Q\bar{Q}$ system based on the Lorentz-invariant Bethe-Salpeter equation.

As soon as the ground-state quarkonium wave function is known in the LF frame, one can subsequently determine the corresponding real part of the LF potential $V_{Q\bar{Q}}(z,\vec{r},\alpha)$. Let us consider for simplicity the harmonic oscillatory potential in the $Q\bar{Q}$ RF,

$$V^{HO}_{Q\bar{Q}}(\rho) = \frac{1}{2} m_Q \omega_0^2 \rho^2, \tag{2.15}$$

where $\rho$ is the three-dimensional separation between $Q$ and $\bar{Q}$ and $\omega_0 \approx 0.3$ GeV is the oscillatory frequency. The Schrödinger equation with this potential has an analytical solution leading to the following Gaussian shape of the quarkonium wave function in the RF:

$$\Psi^{HO}_V(\rho) = N_{HO} \cdot \exp\left[-\frac{1}{4} m_Q \omega_0 \rho^2\right], \tag{2.16}$$

where $N_{HO}$ is the normalization factor such that $\int d^3\rho |\Psi^{HO}(\rho)|^2 = 1$.

Applying the recipe from Ref. [43], as a result of the transition from the nonrelativistic $Q\bar{Q}$ rest frame to the LF frame, one can obtain the following LF counterpart [8,9] of $\Psi^{HO}_V(\rho)$:

$$\Psi^{HO}_V(\vec{r},\alpha) = C\alpha(1-\alpha) f(\alpha) \exp\left[-\frac{1}{2} a^2(\alpha) r^2\right] \tag{2.17}$$

with

$$f(\alpha) = \exp\left[-\frac{m_Q^2}{2a^2(\alpha)} + \frac{4\alpha(1-\alpha)m_Q^2}{2a^2(\alpha)}\right], \tag{2.18}$$

and

$$a^2(\alpha) = \omega_0 m_q 4\alpha(1-\alpha)/2 = a_1^2 4\alpha(1-\alpha), \tag{2.19}$$

keeping the normalization condition $\int d^2 r d\alpha |\Psi^{HO}_V(\vec{r},\alpha)|^2 = 1$.

In order to find the real part of the LF potential $V^{HO}_{Q\bar{Q}}(z,\vec{r},\alpha)$ in the LF frame, the wave function (2.17) should satisfy the following Schrödinger equation:

$$\left(\frac{a^2(\alpha)-\Delta_r}{2k\alpha(1-\alpha)} + \mathcal{R}eV^{HO}_{Q\bar{Q}}(z,\vec{r},\alpha)\right)\Psi^{HO}_V(\vec{r},\alpha) = E^{HO}_{LF} \cdot \Psi^{HO}_V(\vec{r},\alpha), \tag{2.20}$$

with the corresponding eigenvalue $E^{HO}_{LF} = 3a^2(\alpha)/(2k\alpha(1-\alpha))$. This equation can be solved analytically giving the following form of $\mathcal{R}eV_{Q\bar{Q}}(z,\vec{r},\alpha)$ [22]:

$$\mathcal{R}eV_{Q\bar{Q}}(z,\vec{r},\alpha) = \frac{a^4(\alpha) r^2}{2k\alpha(1-\alpha)}. \tag{2.21}$$

Indeed, such a real part of the LF potential was used in Refs. [9,10,12] for the study of shadowing and absorption phenomena in vector meson electroproduction off nuclear targets within a rigorous Green function formalism. The shape of the LF wave function in Eq. (2.17) guarantees a correct nonrelativistic limit ($\alpha \to 0.5$, $\vec{r} \to \vec{\rho}$) of the LF potential, Eq. (2.21), leading to the HO form in the RF given by Eq. (2.15).

Considering now an arbitrary model for $Q$-$\bar{Q}$ interaction potential in the $Q\bar{Q}$ RF, one can obtain $\mathcal{R}eV_{Q\bar{Q}}(z,\vec{r},\alpha)$ in the LF frame only numerically as a solution of the following Schrödinger equation, which is similar to Eq. (2.20),

$$\left(\frac{A^2(\alpha)-\Delta_r}{2k\alpha(1-\alpha)} + \mathcal{R}eV_{Q\bar{Q}}(z,\vec{r},\alpha)\right)\Psi_V(\vec{r},\alpha) = E_{LF} \cdot \Psi_V(\vec{r},\alpha), \tag{2.22}$$

where the LF potential including the term with function $A^2(\alpha)$ can be written as

$$\begin{aligned}\mathcal{R}eV^*_{Q\bar{Q}}(z,\vec{r},\alpha) &= \mathcal{R}eV_{Q\bar{Q}}(z,\vec{r},\alpha) + \frac{A^2(\alpha)}{2k\alpha(1-\alpha)} \\ &= E_{LF} + \frac{1}{\Psi_V(\vec{r},\alpha)} \cdot \frac{\Delta_r \Psi_V(\vec{r},\alpha)}{2k\alpha(1-\alpha)}.\end{aligned} \tag{2.23}$$

In analogy with the HO potential, the function $A^2(\alpha) = A_1^2 4\alpha(1-\alpha)$ and the factor $A_1^2$ can be determined from the nonrelativistic limit ($\vec{r} \to \vec{\rho}, \alpha \to 0.5$) of Eq. (2.22),

$$A_1^2 = m_Q[E_{RF} - V_{Q\bar{Q}}(\vec{\rho})] + \frac{\Delta_r \Psi_V(\vec{r} \to \vec{\rho}, \alpha \to 0.5)}{\Psi_V(\vec{r} \to \vec{\rho}, \alpha \to 0.5)}, \tag{2.24}$$

where $V_{Q\bar{Q}}(\vec{\rho})$ is the quark interaction potential in the $Q\bar{Q}$ rest frame and the eigenvalue $E_{RF}$ is related to that in the LF frame via relation,

$$E_{LF} = E_{RF} \cdot \frac{m_Q 4\alpha(1-\alpha)}{2k\alpha(1-\alpha)}. \tag{2.25}$$

Finally, the LF potential for any model describing the $Q$-$\bar{Q}$ interaction in the RF can be obtained from the following relation:

$$\mathcal{R}eV_{Q\bar{Q}}(\vec{r},\alpha) = E_{LF} + \frac{1}{\Psi_V(\vec{r},\alpha)}\cdot\frac{\Delta_r\Psi_V(\vec{r},\alpha)}{2k\alpha(1-\alpha)} - \frac{A_1^2 4\alpha(1-\alpha)}{2k\alpha(1-\alpha)}. \quad (2.26)$$

Taking the analytical form of $\mathcal{R}eV_{Q\bar{Q}}(z_2,\vec{r}_2,\alpha)$ given by Eq. (2.21) corresponding to the harmonic oscillatory form (2.15) in the $Q\bar{Q}$ rest frame, the evolution equation (2.7) has an analytical solution, the harmonic oscillator Green function [45]

$$G_{Q\bar{Q}}(z_2,\vec{r}_2;z_1,\vec{r}_1) = \frac{a^2(\alpha)}{2\pi i\sin(\omega\Delta z)}\exp\left\{\frac{ia^2(\alpha)}{2\sin(\omega\Delta z)} \times[(r_1^2+r_2^2)\cos(\omega\Delta z) - 2\vec{r}_1\cdot\vec{r}_2]\right\} \times\exp\left[-\frac{i\eta^2\Delta z}{2k\alpha(1-\alpha)}\right], \quad (2.27)$$

where $\Delta z = z_2 - z_1$ and

$$\omega = \frac{a^2(\alpha)}{k\alpha(1-\alpha)}. \quad (2.28)$$

The boundary condition in Eq. (2.27) is $G_{Q\bar{Q}}(z_2,\vec{r}_2;z_1,\vec{r}_1)|_{z_2=z_1} = \delta^{(2)}(\vec{r}_1-\vec{r}_2)$. For other LF potentials $\mathcal{R}eV_{Q\bar{Q}}(z_2,\vec{r}_2,\alpha)$, corresponding to COR, LOG, POW, and BT models in the $Q\bar{Q}$ rest frame, Eq. (2.7) for the Green function has to be solved only numerically. Note that the LF oscillatory frequency $\omega$ in Eq. (2.28) has a correct nonrelativistic limit $\omega_0$ in the $Q\bar{Q}$ rest frame.

Considering the propagation of an interacting $Q\bar{Q}$ pair in the nuclear medium, the corresponding Green function satisfies the same evolution equation as given by Eq. (2.7). However, the LF potential acquires besides the real part [see e.g., Eq. (2.21) for the HO form of the LF potential] also the imaginary part, which represents an absorption of the $Q\bar{Q}$ Fock state of the photon in the medium,

$$\mathcal{I}mV_{Q\bar{Q}}(z_2,\vec{r},\alpha) = -\frac{\sigma_{Q\bar{Q}}(\vec{r},s)}{2}\rho_A(b,z_2). \quad (2.29)$$

Such form of the LF potential was used in Refs. [13,23,46–48] for calculation of nuclear shadowing in deep-inelastic scattering off nuclei in a good agreement with data.

In order to keep the analytical solution of Eq. (2.7), the whole LF potential $V_{Q\bar{Q}}(z_2,\vec{r}_2,\alpha)$ should acquire the HO form, i.e., the imaginary part given by Eq. (2.29) should be proportional to $r^2$ as well. This requires to employ the quadratic $r$-dependence of the dipole cross section

$$\sigma_{Q\bar{Q}}(r,s) = C(s)r^2. \quad (2.30)$$

Such an approximation has a reasonable good accuracy for heavy quarkonium photoproduction and electroproduction due to sufficiently small $Q$-$\bar{Q}$ dipole sizes contributing to production amplitudes. However, instead of the approximation (2.30), in the present paper we adopt two realistic phenomenological parametrizations for $\sigma_{Q\bar{Q}}(r,s)$ of the saturated form. Model predictions with the parametrization for $\sigma_{Q\bar{Q}}(r,s)$ from Ref. [49] within the known Golec-Biernat-Wushoff (GBW) model [50,51] will be compared with results based on Kopeliovich-Schafer-Tarasov (KST) model [22], extended for the additional Reggeon term as given in Ref. [9].

Note that the relevance of $\mathcal{R}eV_{Q\bar{Q}}$ in calculations of charmonium yields gradually decreases with the photon energy as one can see from Eq. (2.26). Consequently, the modification of $d\sigma/dy$ related to $\mathcal{R}eV_{Q\bar{Q}}$ manifests itself only at large forward and/or backward rapidities and is more visible at smaller RHIC energies compared to the LHC kinematic region. In Fig. 1, we compare model predictions based on the path integral technique at c.m. collision energy $\sqrt{s_N} = 200$ GeV neglecting (dashed lines) and including (solid lines) $\mathcal{R}eV_{Q\bar{Q}}$. One can see that the importance of $\mathcal{R}eV_{Q\bar{Q}}$ gradually decreases towards the midrapidity region $y = 0$. Whereas for the coherent $J/\psi(1S)$ production in UPC the additional incorporation of $\mathcal{R}eV_{Q\bar{Q}}$ enhances $d\sigma/dy$, the nodal structure of the $\psi'(2S)$ wave function leads to a counterintuitive reduction of $d\sigma/dy$.

### C. Nuclear production amplitudes incorporating Melosh spin effects

Terent'ev boosting prescription [43] to the LF frame requires a significant correction [30] due to transverse motion of the quarks when their momenta are not parallel to the boost axis. This leads to quark spin rotation effects known also as the Melosh spin effects [55] that have been included in our calculations following Refs. [14,17,56]. We also ruled out the photonlike vertex for a heavy quarkonium transition $V \to Q\bar{Q}$ pair due to abnormally large weight of a $D$-wave component, as analyzed in Ref. [14].

In this paper, we have adopted the structure of the $V \to Q\bar{Q}$ vertex from our previous studies in Refs. [11,14,16,17,57]. Then, assuming $s$-channel helicity conservation, the final expression for the coherent amplitude including the Melosh spin rotation is given again by Eq. (2.5) but with the function $H_1(s,b,z)$ of the following form

$$H_1^{T,L}(s,b,z) = \int_0^1 d\alpha\int d^2r_1 d^2r_2 G_{Q\bar{Q}}(z',\vec{r}_2;z,\vec{r}_1)\Big|_{z'\to\infty} \cdot\Omega_{T,L}(r_1,r_2,\alpha)\cdot\sigma_{Q\bar{Q}}(r_1,s), \quad (2.31)$$

where $\Omega_T(r_1,r_2,\alpha) = \Sigma_T^{(1)}(r_1,r_2,\alpha) + \Sigma_T^{(2)}(r_1,r_2,\alpha)$ and $\Omega_L(r_1,r_2,\alpha) = \Sigma_L(r_1,r_2,\alpha)$ for transversely (T) and longitudinally (L) polarized photon and quarkonium,

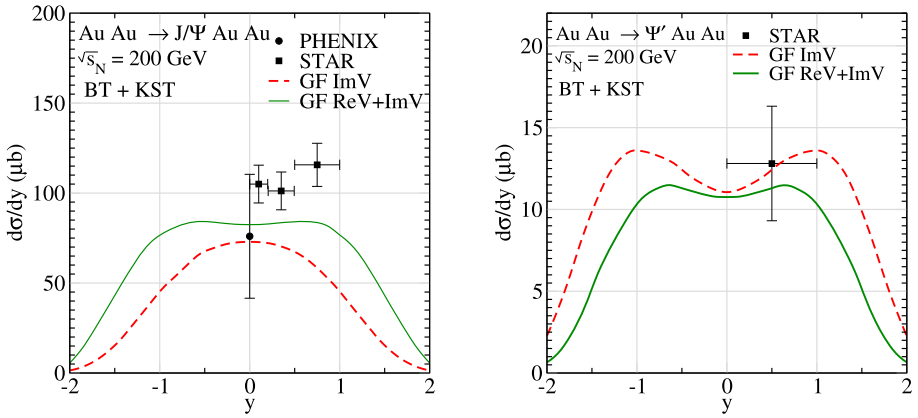


FIG. 1. The impact of $\mathcal{R}eV_{Q\bar{Q}}$ on rapidity distribution $d\sigma/dy$ for coherent $J/\psi(1S)$ (left panel) and $\psi'(2S)$ (right panel) production in UPC at c.m. collision energy $\sqrt{s_N} = 200$ GeV. Values of $d\sigma/dy$ are calculated within the Green function formalism adopting the BT $Q$-$\bar{Q}$ interaction potential and KST model for dipole cross section. Dashed and solid lines correspond to the case when $\mathcal{R}eV_{Q\bar{Q}}$ is neglected and included in model predictions, respectively. The data are from the PHENIX [52] and STAR [53,54] experiments.

respectively. Treating charmonium electroproduction, one can safely consider, with a rather good accuracy, the perturbative wave functions for the incoming photon, $\Psi_{\gamma(\gamma^*)}(\vec{r},\alpha) = K_0(\eta r)$. Then the functions $\Sigma_T^{(1,2)}$ and $\Sigma_L$ read

$$\Sigma_T^{(1,2)}(r_1,r_2,\alpha) = NK_{0,1}(\eta r_1)\int_0^\infty dp_T p_T J_{0,1}(p_T r_2) \times \Psi_V(p_T,\alpha)\mathcal{R}_T^{(1,2)}(p_T) \tag{2.32}$$

with

$$\mathcal{R}_T^{(1)}(p_T) = \frac{2m_Q^2(m_L+m_T)+m_L p_T^2}{m_T(m_L+m_T)},$$
$$\mathcal{R}_T^{(2)}(p_T) = \frac{m_Q^2(m_L+2m_T)-m_T m_L^2}{m_Q^2 m_T(m_L+m_T)}\eta p_T, \tag{2.33}$$

and

$$\Sigma_L(r_1,r_2,\alpha) = NK_0(\eta r_1)\int_0^\infty dp_T p_T J_0(p_T r_2) \times \Psi_V(p_T,\alpha)\mathcal{R}_L(p_T) \tag{2.34}$$

with

$$\mathcal{R}_L(p_T) = 4Q\alpha(1-\alpha)\frac{m_Q^2+m_L m_T}{m_Q(m_L+m_T)}. \tag{2.35}$$

Here $N = Z_Q\sqrt{2N_c\alpha_{em}}/4\pi$, where the factor $N_c = 3$ represents the number of colors in QCD, $Z_Q = \frac{2}{3}$ is the charge-isospin factor for the production of charmonia, and $J_{0,1}$ are the Bessel functions of the first kind. The variables $m_{T,L}$ in Eqs. (2.33) and (2.35) have the following form:

$$m_T = \sqrt{m_Q^2+p_T^2}, \quad m_L = 2m_Q\sqrt{\alpha(1-\alpha)}. \tag{2.36}$$

The magnitude of the charm quark mass corresponds to values from the realistic phenomenological models for the $c-\bar{c}$ interaction potential, such as POW and BT, used in our analysis.

Finally, the total cross section (2.3) can be expressed as the sum of T and L contributions

$$\sigma_A^{coh}(s) = \sigma_{A,T}^{coh}(s) + \tilde{\varepsilon}\sigma_{A,L}^{coh}(s), \tag{2.37}$$

where we have taken the photon polarization $\tilde{\varepsilon} = 1$.

### D. Gluon shadowing

It was shown in Refs. [15,57] that heavy quarkonia produced in photo-nuclear reactions in UPC are affected mainly by two specific nuclear effects; the gluon shadowing (GS) and the effect of reduced coherence length when $l_c \lesssim R_A$. Whereas the later effect is naturally incorporated in the Green function formalism described in Sec. II A, the effects of GS have to be included additionally as a shadowing correction corresponding to higher Fock components of the photon containing gluons, i.e., $|Q\bar{Q}G\rangle, |Q\bar{Q}2G\rangle \ldots |Q\bar{Q}nG\rangle$.

The leading twist gluon shadowing was introduced in Ref. [22] within the dipole representation. We have demonstrated in Refs. [9–12] that such effect substantially modifies cross sections at high energies in photoproduction of vector mesons on nuclei. According to analysis and discussion in Ref. [14], only the one-gluon Fock state $|Q\bar{Q}G\rangle$ of the photon gives a dominant contribution to the

nuclear shadowing within the kinematic regions of present UPC experiments at the LHC.

We have incorporated the GS correction in our calculations as a reduction of $\sigma_{Q\bar{Q}}(r,s)$ in nuclear reactions with respect to processes on the nucleon [58],

$$\sigma_{Q\bar{Q}}(r,x) \Rightarrow \sigma_{Q\bar{Q}}(r,x)\cdot R_G(x,b), \tag{2.38}$$

where the correction factor $R_G(x,b)$ related to the $Q\bar{Q}G$ component of the photon, was calculated within the Green function formalism as a function of the nuclear impact parameter $b$ and variable $x$, in analogy with our previous works [9–11,13,22,23,58] (see also Fig. 1 and discussion in Ref. [14]).

## III. MODEL PREDICTIONS VS AVAILABLE DATA

We calculated the coherent charmonium photoproduction in UPC according to Eq. (2.1), as well as electroproduction at EIC energies using Eqs. (2.3) and (2.37). The corresponding nuclear cross sections are obtained within a rigorous Green function formalism as described in Sec. II A. The evolution equation, Eq. (2.7), for the Green function is solved numerically following the algorithm from Ref. [48]. The Melosh spin transformation is included as specified in Sec. II C. Besides effects of the quantum coherence for the lowest $|Q\bar{Q}\rangle$ Fock state of the photon, we included also the leading twist gluon shadowing corrections (see Sec. II D) in our calculations at large photon energies.

In Fig. 2, we present a comparison of our model predictions for the rapidity distributions $d\sigma/dy$ of coherent $J/\psi(1S)$ (left panels) and $\psi'(2S)$ (right panels) photoproduction in UPC with available data covering a broad spectrum of c.m. collision energies, $\sqrt{s_N} = 200$ GeV (top panels), $\sqrt{s_N} = 2.76$ TeV (middle panels) and $\sqrt{s_N} = 5.02$ TeV (bottom panels). Our results were obtained for charmonium wave functions generated by two distinct $Q$-$\bar{Q}$ interaction potentials, POW (dotted and dot-dashed lines) and BT (solid and dashed lines). For the dipole cross sections $\sigma_{Q\bar{Q}}$ we used GBW (solid and dot-dashed lines) and KST (dashed and dotted lines) parametrizations.

Figure 2 shows a rather good agreement of our predictions based on the Green function formalism with data at all collision energies. The best description of data is achieved with the charmonium wave function generated by the POW $c-\bar{c}$ potential combined with the GBW model for $\sigma_{Q\bar{Q}}$ and/or by the BT $c-\bar{c}$ potential combined with the KST model for $\sigma_{Q\bar{Q}}$. The values of $d\sigma/dy$ strongly depend on the shape of the 1S-charmonium wave function. Such an observation is consistent with our previous studies [16] of quarkonium electroproduction off protons. On the other hand, taking into account the latest GBW parametrization of $\sigma_{Q\bar{Q}}(r,x)$ from [49], the corresponding calculations lead to magnitudes of $d\sigma/dy$ exhibiting quite large deviation from values based on the KST model for $\sigma_{Q\bar{Q}}(r,x)$.

Investigation of radially excited charmonia can provide us with an additional information about the photoproduction mechanisms in UPC due to the nodal structure of their radial wave functions. Such wave functions are more sensitive to the shape of the $c-\bar{c}$ interaction potential compared to 1S-charmonium state (see Fig. 3 in Ref. [16]). However, the model predictions for $d\sigma/dy$ and $\psi'(2S)$ production, shown in the right panels of Fig. 2, exhibit much weaker sensitivity to the shape of the potential. In fact, there are large differences in $d\sigma/dy$ related to the model for $\sigma_{Q\bar{Q}}$. Thus, the measurements of exclusive electroproduction of radially excited charmonia in nuclear UPC may provide additional constraints on the models for dipole cross section.

Figure 3 demonstrates how particular nuclear effects modify the rapidity distribution $d\sigma/dy$ at the collision energy $\sqrt{s_N} = 5.5$ TeV, which is planned to be measured at the LHC. Here the left and right panels present model calculations including BT and POW $c-\bar{c}$ interaction potential in combination with the KST and GBW parametrization for $\sigma_{Q\bar{Q}}$, respectively. Top and bottom panels correspond to model predictions for 1S and 2S charmonium states, respectively. Whereas dashed lines are related to calculations in the high-energy eikonal approximation, $l_c \gg R_A$ [see Eq. (2.14)] without corrections to finite coherence length and GS, the solid lines were obtained within the Green function formalism [see Eqs. (2.5) and (2.6)], accounting also for the leading twist GS effects. The differences between the solid and dotted lines are caused by the leading twist GS at midrapidities and by the reduced effects of higher-twist quark shadowing at forward/backward rapidities.

Following discussion in Sec. V. H. of Ref. [16] we avoided the skewness effect in all calculations due to an absence of the exact analytical expression for the correction factor $R_g(\Lambda)$ in the literature. The approximate relation for $R_g(\Lambda)$ from Ref. [68] is based on several assumptions, such as the strong inequalities $x' \ll x \ll 1$[1] and the specific power-law form of the diagonal gluon density of the target. This does not allow its application for all kinematic regions covered by recent UPC experiments. Nevertheless, the formal implementation of the skewness correction from Ref. [68] increases the magnitude of $d\sigma/dy$ by a factor of $\sim 1.4 \div 1.5$ for $J/\psi(1S)$ and by $\sim 1.7 \div 2.0$ for $\psi'(2S)$ production. However, it does not lead to any sizeable effect in calculations of nuclear modification factors $R_A^{coh}$ given by Eq. (3.1).

The sophisticated path integral method may significantly improve model predictions in the kinematic region where

[1]Variables $x$ and $x'$ are the LF fractions of the proton momentum carried by the gluons attached to the $Q\bar{Q}$ fluctuation of the photon.

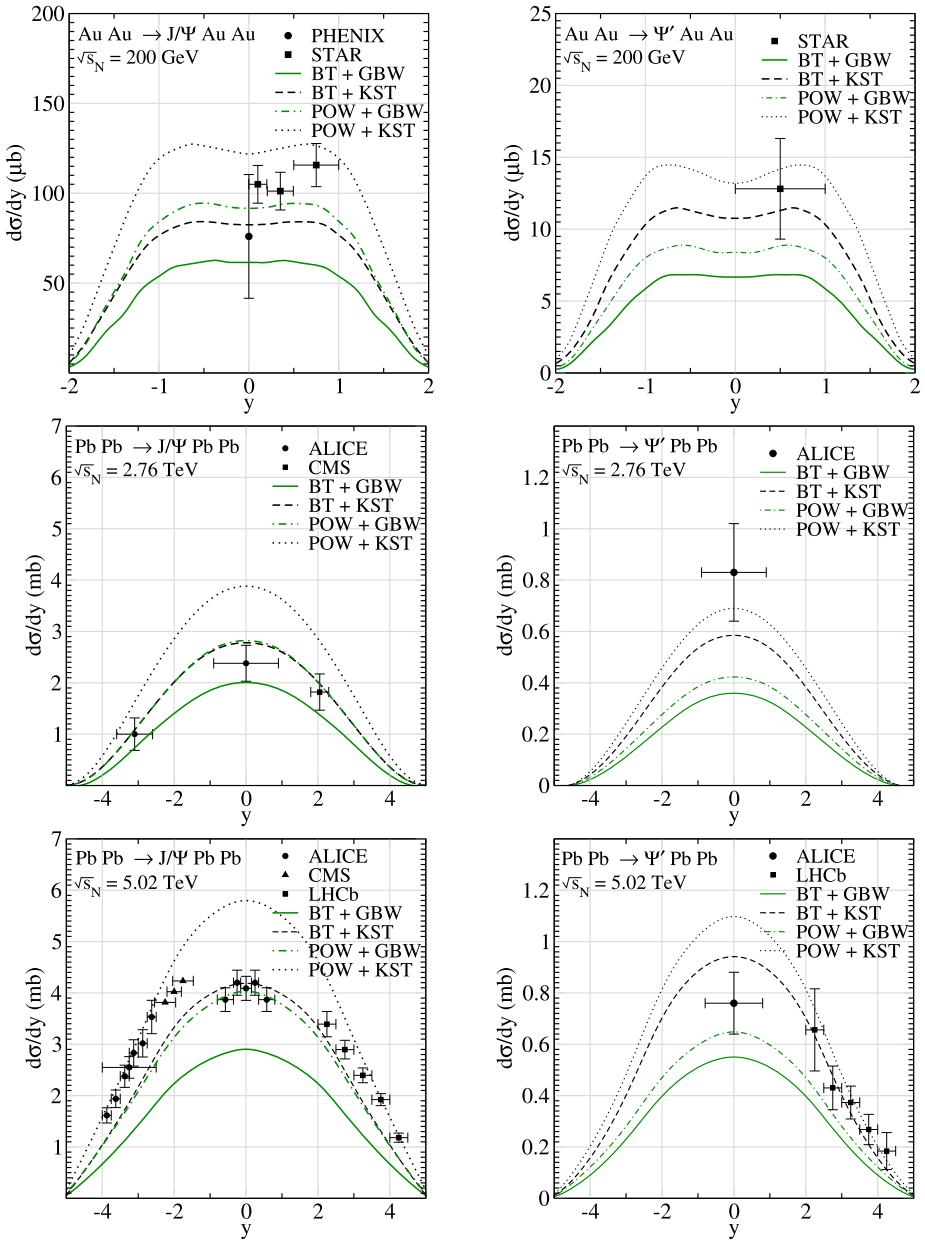


FIG. 2. Rapidity distributions of coherent $J/\psi(1S)$ (left panels) and $\psi'(2S)$ (right panels) photoproduction in UPC at RHIC collision energy $\sqrt{s_N} = 200$ GeV (top panels) and at LHC energies $\sqrt{s_N} = 2.76$ TeV (middle panels), and $\sqrt{s_N} = 5.02$ TeV (bottom panels). The nuclear cross sections are calculated with charmonium wave functions generated by the POW (dot-dashed and dotted lines) and BT (solid and dashed lines) potentials using GBW (solid and dot-dashed lines) and KST (dashed and dotted lines) models for the dipole cross section. The data for $d\sigma/dy$ from the PHENIX [52], STAR [53,54], CMS [59], ALICE [60–64], LHCb [65,66] and CMS [67] Collaborations are shown for comparison.

$l_c \lesssim R_A$. In Fig. 4, we present a comparison of our previous results from Ref. [15] with calculations based on the Green function formalism at the RHIC collision energy. For 1S charmonium production they differ by about $10 \div 20\%$ at forward/backward rapidities. However, for the coherent production of $\psi'(2S)$, such a comparison exhibits larger difference, by $30 \div 40\%$, due to a nodal structure of the corresponding charmonium wave function and larger averaged size, $\langle r^2_{\psi'} \rangle > \langle r^2_{J/\psi} \rangle$ [30]. We predict similar difference between the present and previous results from Ref. [15] also in the LHC kinematic region related to values of $y$ ($|y| \sim 4 \div 5$) that are effective for manifestation of reduced effects of quantum coherence.

The precise calculations of coherence effects are indispensable for a proper description and interpretation of future data on quarkonium electroproduction from

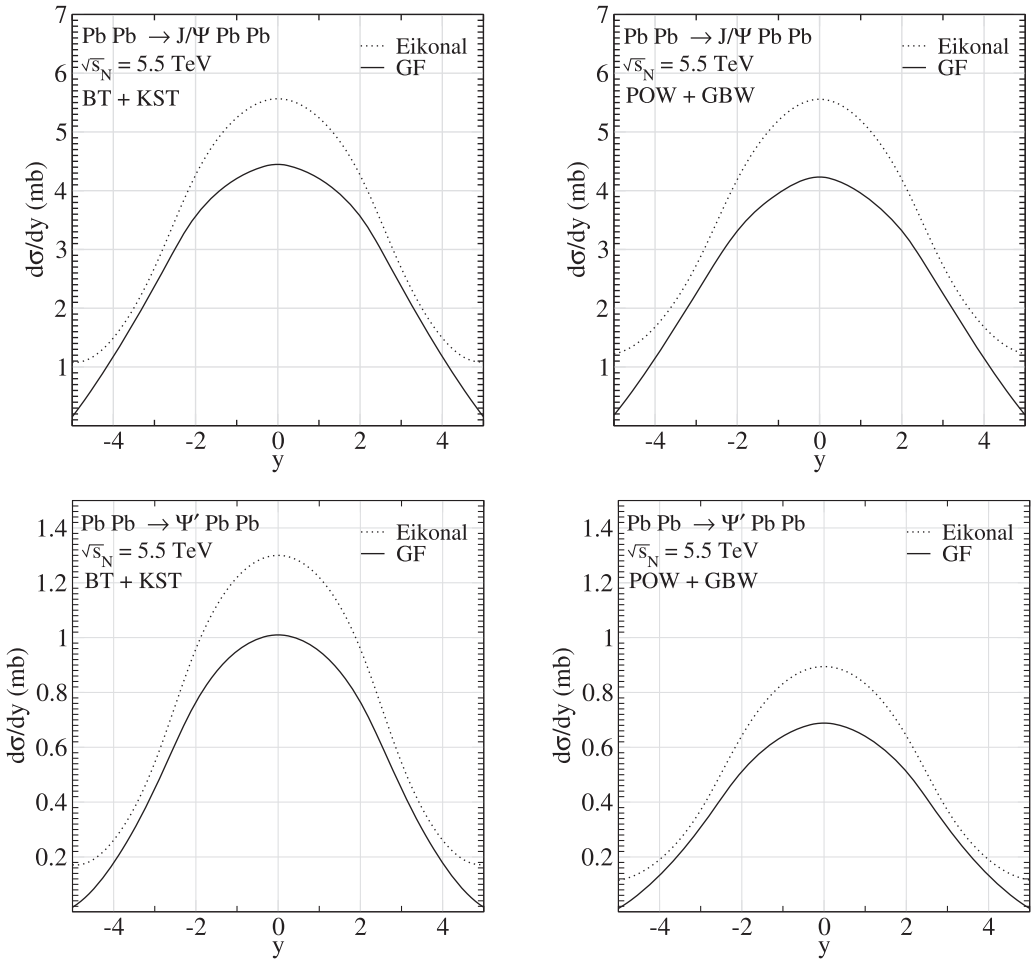


FIG. 3. Manifestations of particular nuclear effects in coherent photoproduction of charmonia in UPC at the LHC collision energy $\sqrt{s_N} = 5.5$ TeV. Top and bottom panels correspond to production of 1S and 2S charmonium states, respectively. The nuclear cross sections are calculated with charmonium wave functions generated by the BT potential adopting the KST model for the dipole cross section (left panels) and by the POW potential combined with the GBW dipole model (right panels). The dotted lines represent predictions in the high-energy eikonal limit, Eq. (2.14). The solid lines are the results of full calculations within the Green function formalism including also the gluon shadowing effects.

measurements at planned EIC, mainly at large photon virtualities, $Q^2 \gg m_Q^2$, where $l_c \lesssim R_A$. Therefore, in Figs. 5 and 6, we demonstrate an unambiguous benefit of a rigorous Green function formalism, which correctly incorporates the higher and leading twist shadowing corrections. Here we provide predictions for the nucleus-to-nucleon ratios (*nuclear transparency*),

$$R_A^{coh}(J/\psi) = \frac{\sigma_{\gamma^* A \to J/\psi A}}{A\sigma_{\gamma^* N \to J/\psi N}} \quad \text{and} \quad R_A^{coh}(\psi') = \frac{\sigma_{\gamma^* A \to \psi' A}}{A\sigma_{\gamma^* N \to \psi' N}}, \tag{3.1}$$

as a function of the c.m. energy $W$ and $Q^2 + M_V^2$ [$V = J/\psi(1S)$ and $\psi'(2S)$]. The main advantage of investigation of the elastic charmonium electroproduction is that CL effects cannot mimic CT. This is because the contraction of $l_c$ with $Q^2$ [see Eq. (2.10)] results in an increase of suppression of nuclear transparency, which is an effect opposite to CT. For this reason, the coherent process, $\gamma^* + A \to J/\psi(\psi') + A$, is convenient for study of particular nuclear effects by future measurements at EIC. Since manifestations of reduced CL effects are more visible for heavy nuclei with large radius, we restrict ourselves to predictions on the gold target. The values of $R_A^{coh}$ were obtained using the charmonium LF wave function generated by the POW $c - \bar{c}$ interaction potential and the GBW model for $\sigma_{Q\bar{Q}}$. Here, due to complexity of calculations within the Green function formalism, instead of the Dokshitzer-Gribov-Lipatov-Altareli-Parisi (DGLAP) improved GBW saturation model from Ref. [49], we used a modification of the standard GBW model as presented also in Ref. [49] with updated parameters from the fit of deep inelastic scattering HERA data covering higher values of the photon virtuality $Q^2 \lesssim 50$ GeV$^2$. We expect that corresponding calculations of the nucleus-to-nucleon ratio $R_A^{coh}$ at large $Q^2$ will not

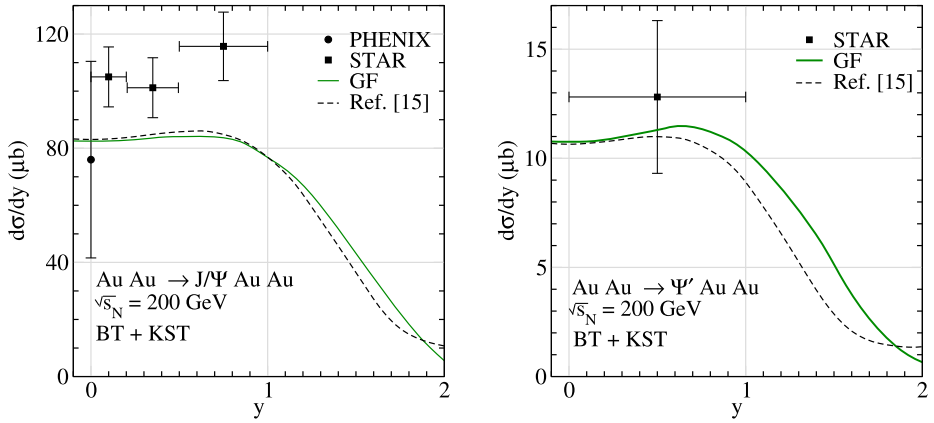


FIG. 4. Rapidity distributions $d\sigma/dy$ of coherent $J/\psi(1S)$ (left panel) and $\psi'(2S)$ (right panel) production in nuclear UPCs at RHIC collision energy $\sqrt{s_N} = 200$ GeV. Present calculations based on path integral technique (solid lines) are compared with our previous results from Ref. [15] (dashed lines). The values of $d\sigma^{coh}/dy$ have been obtained using KST model for $\sigma_{Q\bar{Q}}$ in combination with BT model for $c-\bar{c}$ interaction potential. The data for $d\sigma^{coh}/dy$ from the PHENIX [52] and STAR [53,54] Collaborations are shown for comparison.

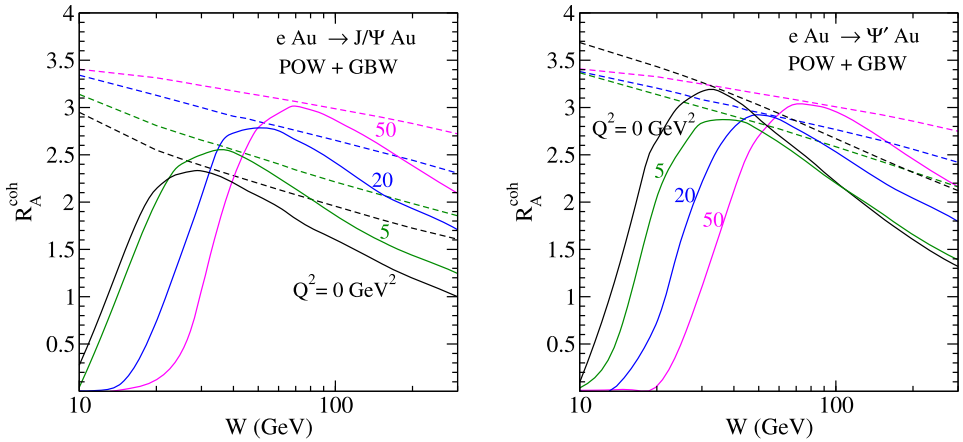


FIG. 5. Ratios $R_A^{coh}$ for the $J/\psi(1S)$ (left panel) and $\psi'(2S)$ (right panel) coherent production on the gold target as function of c.m. energy $W$ at several fixed values of the photon virtuality $Q^2 = 0$ , 5 , 20 , and 50 GeV$^2$. Model predictions are obtained with the GBW parametrization of $\sigma_{Q\bar{Q}}$ and POW model for the $c$-$\bar{c}$ interaction potential. The dashed lines are related to calculations in the high-energy eikonal limit, the solid curves represent the exact calculations within a rigorous Green function formalism including gluon shadowing corrections.

differ much from results based on the DGLAP improved GBW model. Note that the ratio $R_A^{coh} \to A^{1/3}$ at large $Q^2$. For this reason the nuclear modification factor $R_A^{coh}$ exceeds one.

We predict sizable leading twist corrections, rising with the photon energy, that can be seen in Fig. 5 as differences between solid and dashed lines at large $W$. On the other hand, the differences between solid and dashed lines at small and medium photon energies up to the position of maximal values of $R_A^{coh}$ are caused by reduced CL effects, when $l_c \lesssim R_A$ [see Eq. (2.10)]. Here solid lines clearly demonstrate a diminishing of $R_A^{coh}$ towards small photon energies due to suppression of the nuclear coherent cross section by the nuclear form factor, which is properly included in the Green function formalism. At large photon energy, $l_c \gg R_A$ and $R_A^{coh}(W)$ exhibits approximate saturation and then gradual decrease with $W$ due to the increasing value of the dipole cross section with the photon energy. The saturation level is higher at larger $Q^2$ which is a clear manifestation of CT effects. Our predictions for the onset of reduced coherence effects and gluon shadowing can be tested by future experiments at EIC.

Note that model calculations, frequently presented in the literature, are usually performed in the high-energy eikonal limit where the coherence length $l_c$ exceeds considerably the nuclear size, $l_c \gg R_A$. Besides the higher-twist corrections, also the gluon shadowing should be included in the LHC kinematic region where

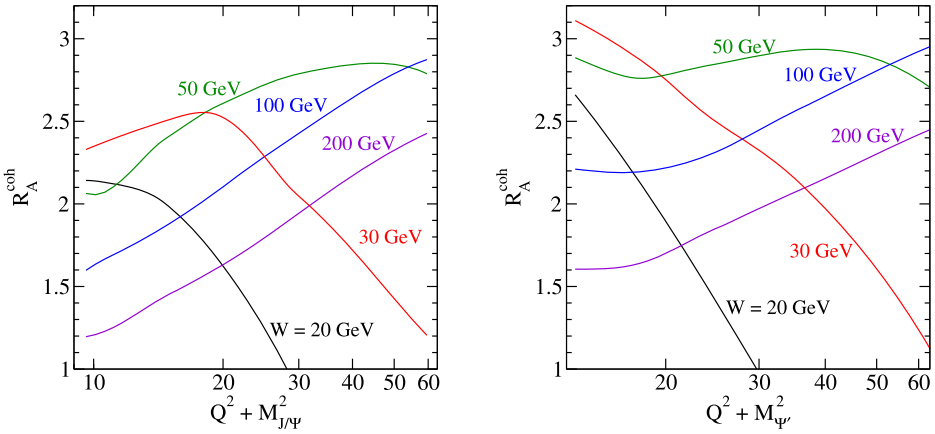


FIG. 6. The same as Fig. 5 but ratios $R_A^{coh}$ are depicted as function of the variable $Q^2 + M^2_{J/\psi}$ (left panel) and $Q^2 + M^2_{\psi'}$ (right panel) at several fixed values of the c.m. photon energy $W = 20$ , 30, 50, 100, and 200 GeV. The lines represent the exact calculations within a rigorous Green function formalism including gluon shadowing corrections.

$l_c^G = l_c/f_G \gg R_A$ with $f_G \approx 10$ found in Ref. [47]. Although such a shadowing correction becomes an important effect at $x \leq 0.01$ [9–12,14,22], it is still missing in the most of recent studies.

In Fig. 6 we investigate how the $Q^2 + M_V^2$-behavior of $R_A^{coh}$ changes at different fixed c.m. energies $W$. At large $W = 100$ and 200 GeV, the coherence length is sufficiently long to neglect its variation with $Q^2 + M_V^2$ and to use the "frozen" approximation. Then the rise of $R_A^{coh}$ with $Q^2$ is a net manifestation of CT effects. However, at smaller photon energies, $W \leq 50$ GeV, $l_c \sim R_A$ and variation of $l_c$ with $Q^2$ [see Eq. (2.10)] causes that the rise of $R_A^{coh}$ gradually slows down and eventually disappears. At $W \leq 20 \div 30$ GeV, $l_c \ll R_A$ and the nuclear transparency $R_A^{coh}$ decreases rapidly with $Q^2$ due to reduced CL effects.

The right panel of Fig. 6 shows a nonmonotonic $Q^2$ behavior of $R_A^{coh}$ at small and medium $Q^2$ at the c.m. energy $W = 50$ GeV, where the variation of $l_c$ with $Q^2$ does not play any role. The node effect causes the rise of the overlap of the $c\bar{c}$ state and the $\psi'(2S)$ wave function with $Q^2$ in the numerator and denominator of $R_A^{coh}$. The nuclear medium filters out large size $c\bar{c}$ configurations with larger absorption cross section. Consequently, the color filtering effect is stronger at smaller $Q^2$ and thus the $Q^2$ squeezing of the transverse size of a $c\bar{c}$ wave packet is less pronounced in the numerator than in the denominator of the ratio $R_A^{coh}$. As a result, the ratio $R_A^{coh}(Q^2)$ for the coherent production of $\psi'$ can decrease at small $Q^2$. This may explain also a nonmonotonic $Q^2$ dependence of an approximate saturation levels (maxima) of $R_A^{coh}(W)$ at small $Q^2$ in coherent production of $\psi'(2S)$, as is demonstrated in the right panel of Fig. 5. At high $Q^2$, however, the size of the $c\bar{c}$ fluctuation is so small that color filtering does not play any role. Then the nuclear medium becomes more transparent for smaller $c\bar{c}$ sizes and may eventually cause a rise of $R_A^{coh}(Q^2)$ with $Q^2$. If the CL still exceeds considerably the nuclear radius, such a rise of $R_A^{coh}(Q^2)$ is a net manifestation of CT effects [see a rise of $R_A^{coh}(Q^2)$ at $W = 50$ , 100 , and 200 GeV at medium and large $Q^2$ in the right panel of Fig. 6].

## IV. CONCLUSIONS

In this paper we present for the first time the comprehensive and uniform quantum-mechanical description of heavy quarkonium production in heavy-ion ultraperipheral and electron-ion collisions based on a rigorous Green function formalism, revising thus our previous results from Ref. [15]. Here we summarize the following main observations:

(i) The coherence length $l_c$ for the lowest $|Q\bar{Q}\rangle$ Fock state of the photon exceeds considerably the nuclear size in UPC at RHIC and the LHC at midrapidities. This enables us to adopt the high-energy eikonal approximation for nuclear effects given by Eq. (2.14). Such an approximation can be reached naturally also within the Green function formalism in the limit of large photon energies as was demonstrated in Sec. II A. The corresponding shadowing correction represents the higher-twist effect, which is small for heavy quarkonia since it vanishes with heavy quark mass as $1/m_Q^2$.

(ii) At forward and/or backward rapidities of UPC kinematics at RHIC and the LHC, the coherence length $l_c \lesssim R_A$ and the eikonalization of $\sigma_{Q\bar{Q}}(r,s)$ cannot be applied anymore for calculations of nuclear cross sections. Here we performed for the first time a rigorous and uniform path-integral-technique description. It does not require to calculate the reduced coherence effects via effective correction factors as was done in Ref. [15]. Moreover, such formalism can be applied without restrictions for the coherence length $l_c$, for arbitrary realistic $Q$-$\bar{Q}$

interaction potential, as well as for any phenomenological model for the dipole cross section and/or impact-parameter-dependent partial dipole amplitude. This represents a substantial improvement of our work [15], modifying our previous results of rapidity distributions $d\sigma/dy$ at small photon energies. For 1S charmonium production they differ by about $10 \div 20\%$ from our present results. However, for $\psi'(2S)$ production they exhibit larger difference, by $30 \div 40\%$, due to the nodal structure of the 2S charmonium wave function.

(iii) We have proposed a procedure how to obtain the real part of potentials $\mathcal{R}eV_{Q\bar{Q}}(z, \vec{r}, \alpha)$ in the LF frame from various realistic models describing the $Q$-$\bar{Q}$ interaction in the rest frame. Such potentials lead to a correct shape of quarkonium wave functions in the LF frame. This is unavoidable for a proper solution of the Schrödinger equation (2.7) for the Green function.

(iv) The higher Fock components of the photon containing gluons lead to gluon shadowing corrections with corresponding coherence length, which is much shorter compared to the lowest $|Q\bar{Q}\rangle$ Fock state. The $|Q\bar{Q}G\rangle$ Fock state of the photon gives the dominant contribution to nuclear shadowing and represents the leading-twist effect due to much larger transverse size of the $Q\bar{Q}$-$G$ dipole compared to the small-sized $Q\bar{Q}$ fluctuation. The gluon shadowing corrections are effective at midrapidities in the LHC kinematic region, reducing considerably the nuclear cross sections $d\sigma/dy$ (see Fig. 3).

(v) Our model predictions have been calculated employing the KST and the latest GBW parametrizations for the dipole cross section $\sigma_{Q\bar{Q}}(r, s)$, as well as BT and POW models for the $Q$-$\bar{Q}$ interaction potential. This provided a possibility to estimate a corresponding measure of the theoretical uncertainty in our current analysis.

(vi) We found a rather good agreement of our revised predictions for $d\sigma/dy$ with available data on coherent production of $J/\psi(1S)$ and $\psi'(2S)$ in UPC at the energies of RHIC and the LHC (see Fig. 2).

(vii) We provided also predictions for the nuclear modification factor $R_A^{coh}$ for coherent charmonium electroproduction as function of the c.m. photon energy $W$ and photon virtuality $Q^2$ in the kinematic regions covered by the future electron-ion collider at RHIC (see Figs. 5 and 6). The leading twist effect causes a rise of the suppression of $R_A^{coh}$ at large photon energies $W$, whereas a vanishing of $R_A^{coh}$ towards small $W$ is caused by the reduced coherence effects (see differences between solid and dashed lines in Fig. 5).

(viii) Investigation of $R_A^{coh}(Q^2)$ by experiments at EIC is very effective for study of particular nuclear phenomena, such as CT and CL effects. Signal of CT may be visible as a rise of nuclear transparency with $Q^2$ at large $W$, where the variation of $l_c$ with $Q^2$ is not important (see Fig. 6). However, the reduced CL effect causes a decrease in $R_A^{coh}(Q^2)$ with $Q^2$ and so do not mimic CT. Thus the onset of the former effect may lead to a significant modification of $R_A^{coh}(Q^2)$ and to a complete elimination of any CT signal at medium energies. Then a strong reduction of $R_A^{coh}$ with $Q^2$ is a clear manifestation of the dominance of reduced CL effect (see lines at $W = 20$ and 30 GeV in Fig. 6).

(ix) The precise calculations of the shadowing and absorption effects in the nuclear medium within a rigorous Green function formalism may be indispensable for the future conclusive evidence of expected gluon saturation effects at large energies.

## ACKNOWLEDGMENTS

The work of J. N. was partially supported by the Slovak Funding Agency, Grant No. 2/0020/22. Computational resources were provided by the e-INFRA CZ project (ID:90254), supported by the Ministry of Education, Youth and Sports of the Czech Republic.

[1] Abdul R. Khalek *et al.*, Science requirements and detector concepts for the electron-ion collider: EIC Yellow Report, Nucl. Phys. **A1026**, 122447 (2022).

[2] J. Adam *et al.* (ATHENA Collaboration), ATHENA detector proposal—a totally hermetic electron nucleus apparatus proposed for IP6 at the Electron-Ion Collider, J. Instrum. **17**, P10019 (2022).

[3] B. Z. Kopeliovich and B. G. Zakharov, Quantum effects and color transparency in charmonium photoproduction on nuclei, Phys. Rev. D **44**, 3466 (1991).

[4] B. Kopeliovich, J. Nemchick, N. N. Nikolaev, and B. Zakharov, Novel color transparency effect: Scanning the wave function of vector mesons, Phys. Lett. B **309**, 179 (1993).

[5] B. Z. Kopeliovich, J. Nemchik, N. N. Nikolaev, and B. G. Zakharov, Decisive test of color transparency in exclusive electroproduction of vector mesons, Phys. Lett. B **324**, 469 (1994).

[6] J. Nemchik, N. N. Nikolaev, and B. Zakharov, Anomalous a-dependence of diffractive leptoproduction of radial excitation $\rho\prime(2s)$, Phys. Lett. B **339**, 194 (1994).

[7] J. Nemchik, N. N. Nikolaev, E. Predazzi, and B. Zakharov, Color dipole systematics of diffractive photoproduction and electroproduction of vector mesons, Phys. Lett. B **374**, 199 (1996).

[8] J. Nemchik, N. N. Nikolaev, E. Predazzi, and B. Zakharov, Color dipole phenomenology of diffractive electroproduction of light vector mesons at HERA, Z. Phys. C **75**, 71 (1997).

[9] B. Kopeliovich, J. Nemchik, A. Schafer, and A. Tarasov, Color transparency versus quantum coherence in electroproduction of vector mesons off nuclei, Phys. Rev. C **65**, 035201 (2002).

[10] J. Nemchik, Incoherent production of charmonia off nuclei as a good tool for study of color transparency, Phys. Rev. C **66**, 045204 (2002).

[11] Y. Ivanov, B. Kopeliovich, A. Tarasov, and J. Hufner, Electroproduction of charmonia off nuclei, Phys. Rev. C **66**, 024903 (2002).

[12] B. Kopeliovich, J. Nemchik, and I. Schmidt, Production of polarized vector mesons off nuclei, Phys. Rev. C **76**, 025210 (2007).

[13] B. Kopeliovich, J. Nemchik, I. Potashnikova, and I. Schmidt, Gluon shadowing in DIS off nuclei, J. Phys. G **35**, 115010 (2008).

[14] B. Z. Kopeliovich, M. Krelina, J. Nemchik, and I. K. Potashnikova, Coherent photoproduction of heavy quarkonia on nuclei, Phys. Rev. D **105**, 054023 (2022).

[15] B. Z. Kopeliovich, M. Krelina, J. Nemchik, and I. K. Potashnikova, Ultraperipheral nuclear collisions as a source of heavy quarkonia, Phys. Rev. D **107**, 054005 (2023).

[16] J. Cepila, J. Nemchik, M. Krelina, and R. Pasechnik, Theoretical uncertainties in exclusive electroproduction of S-wave heavy quarkonia, Eur. Phys. J. C **79**, 495 (2019).

[17] M. Krelina, J. Nemchik, R. Pasechnik, and J. Cepila, Spin rotation effects in diffractive electroproduction of heavy quarkonia, Eur. Phys. J. C **79**, 154 (2019).

[18] M. Krelina, J. Nemchik, and R. Pasechnik, $D$-wave effects in diffractive electroproduction of heavy quarkonia from the photon-like $V \to Q\bar{Q}$ transition, Eur. Phys. J. C **80**, 92 (2020).

[19] I. P. Ivanov, N. N. Nikolaev, and A. A. Savin, Diffractive vector meson production at HERA: From soft to hard QCD, Phys. Part. Nucl. **37**, 1 (2006).

[20] N. Brambilla *et al.* (Quarkonium Working Group), Heavy quarkonium physics, Report No. ERN-2005-005; CERN-2005-005, CERN, Geneva, 2005.

[21] N. Brambilla *et al.*, Heavy quarkonium: Progress, puzzles, and opportunities, Eur. Phys. J. C **71**, 1534 (2011).

[22] B. Z. Kopeliovich, A. Schafer, and A. V. Tarasov, Nonperturbative effects in gluon radiation and photoproduction of quark pairs, Phys. Rev. D **62**, 054022 (2000).

[23] M. Krelina and J. Nemchik, Nuclear shadowing in DIS at electron-ion colliders, Eur. Phys. J. Plus **135**, 444 (2020).

[24] Y. V. Kovchegov, H. Sun, and Z. Tu, Novel cross section ratios as possible signals of saturation in UPCs, Phys. Rev. D **109**, 094028 (2024).

[25] J. Cepila, J. G. Contreras, and M. Krelina, Coherent and incoherent $J/\psi$ photonuclear production in an energy-dependent hot-spot model, Phys. Rev. C **97**, 024901 (2018).

[26] C. Henkels, E. G. de Oliveira, R. Pasechnik, and H. Trebien, Coherent photoproduction of light vector mesons off nuclear targets in the dipole picture, arXiv:2310.06965.

[27] H. Mäntysaari and J. Penttala, Complete calculation of exclusive heavy vector meson production at next-to-leading order in the dipole picture, J. High Energy Phys. 08 (2022) 247.

[28] K. J. Eskola, C. A. Flett, V. Guzey, T. Löytäinen, and H. Paukkunen, Next-to-leading order perturbative QCD predictions for exclusive $J/\psi$ photoproduction in oxygen-oxygen and lead-lead collisions at energies available at the CERN Large Hadron Collider, Phys. Rev. C **107**, 044912 (2023).

[29] C. A. Bertulani, S. R. Klein, and J. Nystrand, Physics of ultra-peripheral nuclear collisions, Annu. Rev. Nucl. Part. Sci. **55**, 271 (2005).

[30] J. Hufner, Y. P. Ivanov, B. Z. Kopeliovich, and A. V. Tarasov, Photoproduction of charmonia and total charmonium proton cross-sections, Phys. Rev. D **62**, 094022 (2000).

[31] H. De Vries, C. W. De Jager, and C. De Vries, Nuclear charge and magnetization density distribution parameters from elastic electron scattering, At. Data Nucl. Data Tables **36**, 495 (1987).

[32] J. Nemchik, N. N. Nikolaev, and B. Zakharov, Scanning the BFKL pomeron in elastic production of vector mesons at HERA, Phys. Lett. B **341**, 228 (1994).

[33] J. Nemchik, Wave function of $2S$ radially excited vector mesons from data for diffraction slope, Phys. Rev. D **63**, 074007 (2001).

[34] J. Nemchik, Anomalous t-dependence in diffractive electroproduction of 2S radially excited light vector mesons at HERA, Eur. Phys. J. C **18**, 711 (2001).

[35] J. B. Bronzan, G. L. Kane, and U. P. Sukhatme, Obtaining real parts of scattering amplitudes directly from cross-section data using derivative analyticity relations, Phys. Lett. **49B**, 272 (1974).

[36] J. R. Forshaw, R. Sandapen, and G. Shaw, Color dipoles and $\rho, \varphi$ electroproduction, Phys. Rev. D **69**, 094013 (2004).

[37] E. Eichten, K. Gottfried, T. Kinoshita, K. D. Lane, and T. M. Yan, Charmonium: Comparison with experiment, Phys. Rev. D **21**, 203 (1980).

[38] E. Eichten, K. Gottfried, T. Kinoshita, K. D. Lane, and T. M. Yan, Charmonium: The model, Phys. Rev. D **17**, 3090 (1978); **21**, 313(E) (1980).

[39] C. Quigg and J. L. Rosner, Quarkonium level spacings, Phys. Lett. **71B**, 153 (1977).

[40] A. Martin, A fit of upsilon and charmonium spectra, Phys. Lett. **93B**, 338 (1980).

[41] N. Barik and S. N. Jena, Fine—hyperfine splittings of quarkonium levels in an effective power law potential, Phys. Lett. **97B**, 265 (1980).

[42] W. Buchmuller and S. H. H. Tye, Quarkonia and quantum chromodynamics, Phys. Rev. D **24**, 132 (1981).

[43] M. V. Terentev, On the structure of wave functions of mesons as bound states of relativistic quarks, Sov. J. Nucl. Phys. **24**, 106 (1976) [Yad. Fiz. **24**, 207 (1976)].
[44] B. Z. Kopeliovich, E. Levin, I. Schmidt, and M. Siddikov, Lorentz-boosted description of a heavy quarkonium, Phys. Rev. D **92**, 034023 (2015).
[45] R. P. Feynman and A. R. Gibbs, *Quantum Mechanics and Path Integrals* (McGraw-Hill Book Company, New York, 1965).
[46] B. Kopeliovich, J. Raufeisen, and A. Tarasov, Challenges of nuclear shadowing in DIS, Phys. Lett. B **440**, 151 (1998).
[47] B. Z. Kopeliovich, J. Raufeisen, and A. V. Tarasov, Nuclear shadowing and coherence length for longitudinal and transverse photons, Phys. Rev. C **62**, 035204 (2000).
[48] J. Nemchik, Nuclear shadowing in DIS: Numerical solution of evolution equation for the green function, Phys. Rev. C **68**, 035206 (2003).
[49] K. Golec-Biernat and S. Sapeta, Saturation model of DIS: An update, J. High Energy Phys. 03 (2018) 102.
[50] K. J. Golec-Biernat and M. Wusthoff, Saturation effects in deep inelastic scattering at low $Q^2$ and its implications on diffraction, Phys. Rev. D **59**, 014017 (1998).
[51] K. J. Golec-Biernat and M. Wusthoff, Saturation in diffractive deep inelastic scattering, Phys. Rev. D **60**, 114023 (1999).
[52] S. Afanasiev *et al.* (PHENIX Collaboration), Photoproduction of $J/\psi$ and of high mass $e^+e$ in ultra-peripheral Au + Au collisions at $\sqrt{S_{NN}} = 200$GeV, Phys. Lett. B **679**, 321 (2009).
[53] STAR Collaboration, Observation of strong nuclear suppression in exclusive $J/\psi$ photoproduction in Au + Au ultra-peripheral collisions at RHIC, Phys. Rev. Lett. **133**, 052301 (2024).
[54] STAR Collaboration, Exclusive $J/\psi$, $\psi(2s)$, and $e^+e^-$ pair production in Au + Au ultra-peripheral collisions at RHIC, Phys. Rev. C **110**, 014911 (2024).
[55] H. J. Melosh, Quarks: Currents and constituents, Phys. Rev. D **9**, 1095 (1974).
[56] T. Lappi, H. Mäntysaari, and J. Penttala, Relativistic corrections to the vector meson light front wave function, Phys. Rev. D **102**, 054020 (2020).
[57] Y. Ivanov, B. Kopeliovich, and I. Schmidt, Vector meson production in ultra-peripheral collisions at LHC, arXiv: 0706.1532.
[58] B. Kopeliovich, A. Tarasov, and J. Hufner, Coherence phenomena in charmonium production off nuclei at the energies of RHIC and LHC, Nucl. Phys. **A696**, 669 (2001).
[59] V. Khachatryan *et al.* (CMS Collaboration), Coherent $J/\psi$ photoproduction in ultra-peripheral PbPb collisions at $\sqrt{s_{NN}} = 2.76$ TeV with the CMS experiment, Phys. Lett. B **772**, 489 (2017).
[60] B. Abelev *et al.* (ALICE Collaboration), Coherent $J/\psi$ photoproduction in ultra-peripheral Pb-Pb collisions at $\sqrt{s_{NN}} = 2.76$ TeV, Phys. Lett. B **718**, 1273 (2013).
[61] E. Abbas *et al.* (ALICE Collaboration), Charmonium and $e^+e^-$ pair photoproduction at mid-rapidity in ultra-peripheral Pb-Pb collisions at $\sqrt{s_{\mathrm{NN}}} = 2.76$ TeV, Eur. Phys. J. C **73**, 2617 (2013).
[62] J. Adam *et al.* (ALICE Collaboration), Coherent $\psi(2S)$ photo-production in ultra-peripheral Pb Pb collisions at $\sqrt{s}_{\mathrm{NN}} = 2.76$ TeV, Phys. Lett. B **751**, 358 (2015).
[63] S. Acharya *et al.* (ALICE Collaboration), Coherent $J/\psi$ photoproduction at forward rapidity in ultra-peripheral Pb-Pb collisions at $\sqrt{s_{\mathrm{NN}}} = 5.02$ TeV, Phys. Lett. B **798**, 134926 (2019).
[64] S. Acharya *et al.* (ALICE Collaboration), Coherent $J/\psi$ and $\psi'$ photoproduction at midrapidity in ultra-peripheral Pb-Pb collisions at $\sqrt{s_{\mathrm{NN}}} = 5.02$ TeV, Eur. Phys. J. C **81**, 712 (2021).
[65] A. Bursche (LHCb Collaboration), Study of coherent $J/\psi$ production in lead-lead collisions at $\sqrt{s_{\mathrm{NN}}} = 5$ TeV with the LHCb experiment, Nucl. Phys. **A982**, 247 (2019).
[66] R. Aaij *et al.* (LHCb Collaboration), Study of exclusive photoproduction of charmonium in ultra-peripheral lead-lead collisions, J. High Energy Phys. 06 (2023) 146.
[67] A. Tumasyan *et al.* (CMS Collaboration), Probing small Bjorken-$x$ nuclear gluonic structure via coherent $J/\psi$ photoproduction in ultraperipheral Pb-Pb collisions at $\sqrt{s_{\mathrm{NN}}} = 5.02$TeV, Phys. Rev. Lett. **131**, 262301 (2023).
[68] A. G. Shuvaev, K. J. Golec-Biernat, A. D. Martin, and M. G. Ryskin, Off diagonal distributions fixed by diagonal partons at small $x$ and $\xi$, Phys. Rev. D **60**, 014015 (1999).